Title

Theory of giant magnetoelastic effect in soft systems.

Journal

Science Advances, 11(1)

Authors

Zhou, Yihao
Chen, Guorui
Zhao, Xun
et al.

Publication Date

2025-01-03

DOI

10.1126/sciadv.ads0071

Peer reviewed

MATERIALS SCIENCE

Theory of giant magnetoelastic effect in soft systems

Yihao Zhou†, Guorui Chen†, Xun Zhao†, Trinny Tat, Zhaoqi Duan, Jun Chen*

Having been predominantly observed in rigid metal and metal alloys since 1865, the magnetoelastic effect was recently experimentally discovered in a soft matter system and used as a new working mechanism for energy and health care applications. Here, a theoretical framework is presented and proven to be universally accurate and robust in interpreting the giant magnetoelastic effect across soft systems subjected to various deformation modes, micromagnet concentrations, magnetization profiles, and geometric structures. The theory uncovers substantial, unique magnetoelastic phenomena in soft systems, including the magnetic pole reversal under localized compression. This work lays a firm foundation for an in-depth understanding and practical applications of the giant magnetoelastic effect in soft matter systems.

INTRODUCTION

The magnetoelastic effect is a phenomenon delineating the alternation of a material's magnetic properties in response to applied mechanical stress or strain. Primarily observed in rigid metals and metal alloys, this effect stems from the rotation or reorientation of the magnetic domains upon the application of mechanical loads (*1*, *2*). Because of the inherent rigidity of the material and the substantial force required to reorient the magnetic domains (*3*, *4*), the magnetoelastic effect has primarily been used in applications within civil engineering, particularly in areas such as building vibration control (*5*, *6*). Recently, a giant magnetoelastic effect has been observed in soft systems comprising micromagnets and a polymer matrix (*7*). As a preliminary attempt, this effect has been coupled with magnetic induction (MI) for the invention of soft magnetoelastic generators (MEGs), emerging as a fundamentally new platform technology for a broad spectrum of applications from cellular reprogramming and cardiovascular health monitoring to wind and water flow energy harvesting (*8*–*11*). Despite their potential, a primary unresolved issue surrounding the phenomena of giant magnetoelastic effects pertains to the absence of a comprehensive, universally applicable, and all-encompassing theoretical framework. Such limitation becomes more pronounced when the soft system assumes an arbitrary geometry and exhibits distinctive magnetization patterns and complex architectures.

Modeling of mechanics in magnetic composites accounting for magnetoelastic coupling has a long and checked history from both the microscopic and macroscopic viewpoints (*12*, *13*). For instance, micromechanical models have been formulated on the basis of the consideration of domain orientation, domain boundary movement, spontaneous magnetization, and magnetization hysteresis of the magnetic particles and use the Mori-Tanaka approach for homogenization to obtain the overall response of the composite (*14*–*18*). These models are suitable for modeling the response of rigid magnetic composites but do not account for the large deformability of soft systems. Macroscopic models have been developed either based on the direct approach using the conservation laws of continuum mechanics (*19*–*23*) or based on the energy approach using the extremization of an appropriate potential energy (*19*, *24*–*29*). These existing models are focused on the magnetic-to-mechanical response of magnetic composite with soft magnetic particles and are not applicable to soft systems with permanent magnetizations. Recently, the theory of hard-magnetic soft systems (*30*–*33*) has been developed and has guided the precise design of magnetic soft robotics for neurovascular interventions (*34*–*36*). Nevertheless, these models are mainly focused on the magnetic-to-mechanical response of the soft systems. There remains an imperative necessity for the development and refinement of models specially designed for simulating the magnetoelastic effect (mechanical-to-magnetic responses) in soft systems, in light of the recent advancements in the applications of this effect across various scenarios.

Here, motivated by the modeling of the magnetic-to-mechanical response of soft systems, we present a theoretical framework specifically tailored to elucidate the giant magnetoelastic effect in soft matter systems experiencing diverse deformation modes. The developed model demonstrates a high degree of consistency and robustness across a series of experiments involving soft systems of diverse deformation modes, regardless of their arbitrary shapes, magnetization intensities, magnetization patterns, and architectures. With this theoretical framework, we highlight the inherent diversity as a key feature of the magnetoelastic effect in soft systems and uncover substantial unique magnetoelastic phenomena including the magnetic pole reversal in localized compression and a potentially record-breaking magnetomechanical coupling (MC) factor of 2.6×10^{-7} T Pa^{-1} at the system center. We summarize two critical parameters determining efficient MC in soft systems: the ratio of initial magnetic flux density B_z to shear modulus G (B_z/G) and the system aspect ratio. This theoretical framework revolutionizes the in-depth understanding of the giant magnetoelastic effect in soft systems, establishing a firm foundation for its further applications in energy, health care, and other domains.

RESULTS

The framework

Preliminary definitions

The theoretical framework hinges on treating the soft matter system comprising micromagnets and a polymer matrix as a homogenized, magnetizable, hyperelastic system (Fig. 1A). In this context, the Neo-Hookean model is chosen for the mechanical behavior of the system which is accurate for compressive strain below 30%. System is defined to occupy a volume $V_0 \in \mathbb{R}^3$ in the reference configuration,

Department of Bioengineering, University of California, Los Angeles, Los Angeles, CA 90095, USA.
*Corresponding author. Email: jun.chen@ucla.edu
†These authors contributed equally to this work.

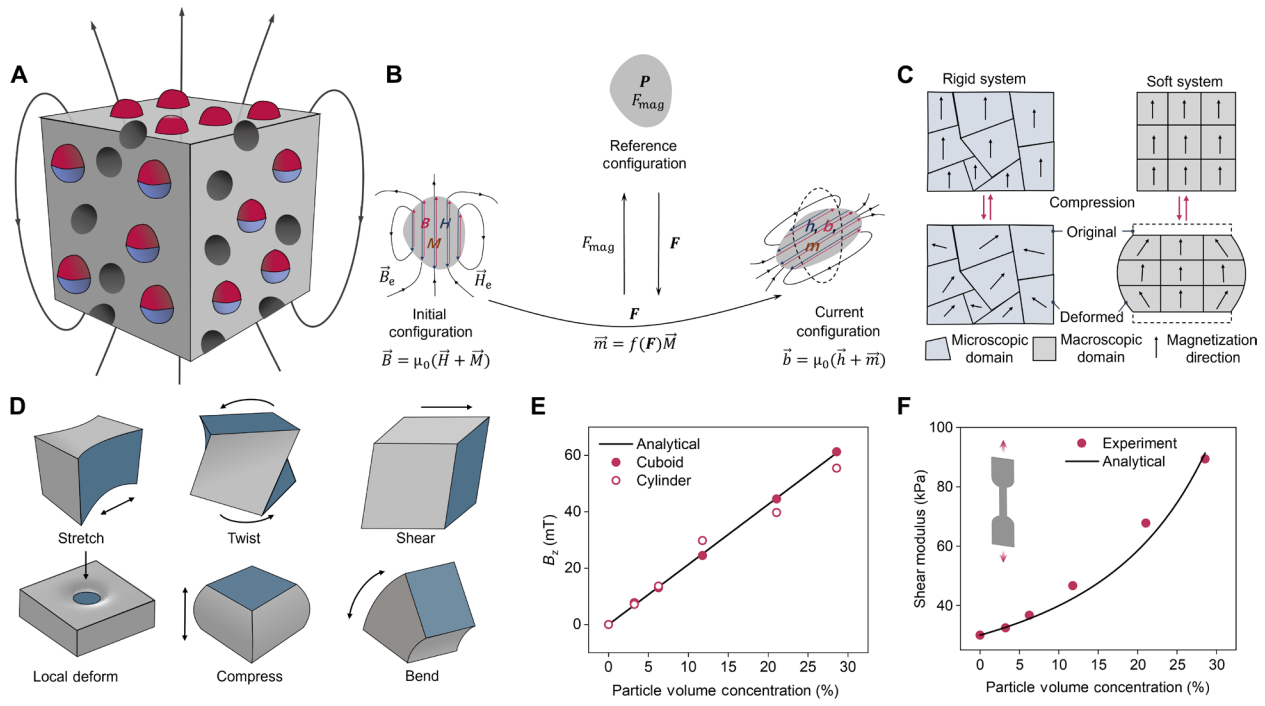

Fig. 1. A theoretical framework to study the magnetoelastic effect in soft systems. (**A**) Scheme of the soft magnetoelastic system composed of oriented micromagnets and a polymer matrix. (**B**) Scheme of the decoupled approach to calculate the giant magnetoelastic effect in soft systems. $\vec{M}$ is related to $\vec{m}$ through $f(\boldsymbol{F})$ to the current configuration. $f(\boldsymbol{F}) = \boldsymbol{R}$ is an appropriate assumption. (**C**) Comparison of rigid and soft systems. (**D**) Different from traditional metals or metal alloys, soft magnetoelastic systems can have different deformation modes ranging from stretch, twist, and shear to compress, bend, and local deform. (**E**) Magnitude of magnetization, represented by the magnetic flux density at the surface center, increases linearly with the particle concentration. (**F**) Shear modulus of the soft magnetoelastic system at different particle concentrations.

with the boundary ∂V_0 and outward unit normal vector $\vec{N}$. Correspondingly, the magnetoelastic soft system is defined to occupy a volume $V \in \mathbb{R}^3$ in the current configuration, with the boundary ∂V and outward unit normal vector $\vec{n}$. The reference and current configurations are linked through a one-to-one deformation map $y(\vec{X})$, with $y(\vec{X}) = \vec{x}$, where $\vec{X} \in V_0$ and $\vec{x} \in V$. Consequently, the deformation gradient is defined as $\boldsymbol{F} = \nabla \vec{x}$. We assume that the deformation of the considered magnetoelastic soft system is isochoric. As a result, the volumetric transformation ratio J, as the determinant of $\boldsymbol{F}$, is consistently equal to 1. Thus, the reference density of the system ρ_0 is equal to the current density ρ. The total second Piola-Kirchhoff stress tensor is denoted as $\boldsymbol{S}$. The Cauchy-Green strain tensor is denoted as $\boldsymbol{C}$. The magnetic flux density, magnetic field, and magnetization in the current configuration are defined as $\vec{b}$, $\vec{h}$, and $\vec{m}$, respectively. The magnetic flux density, magnetic field, and magnetization in the reference configuration are defined as $\vec{B}_r$, $\vec{H}_r$, and $\vec{M}_r$, respectively.

Central concept

We limit the study to an isolated system consisting solely of a permanent magnetic soft object, with no external current sources, no applied magnetic fields, and no interaction with other permanent magnetic objects. In this system, magnetization refers to the remnant magnetization of the system after the impulsed magnetization processes, which is a material parameter. In this system, our theory is built upon the understanding that divergence of magnetization represents the source of Maxwell's equations and can be used to calculate the magnetic field of the system. Thus, variation of the magnetization distribution in the system during deformation can be used to calculate the magnetoelastic effect (fig. S1). According to this understanding, we decouple the calculation of the magnetic part and the mechanical part of the system into two configurations. The mechanical aspect of the problem is addressed within the reference configuration, whereas the magnetic aspect is resolved through the evolution from the initial configuration to the current configuration (Fig. 1B). In this approach, the reference configuration supplies the deformation gradient $\boldsymbol{F}$ for the calculation of the magnetization transformation. Concurrently, the magnetization distribution provides the magnetic force F_{mag}, which is applied as both body and boundary stress to the reference configuration. Consequently, the magnetoelastic coupling is achieved through the exchange of magnetic and mechanical parameters between these two configurations. The magnetic flux density, magnetic field, and magnetization in the initial configuration are defined as $\vec{B}$, $\vec{H}$, and $\vec{M}$, respectively. It is noteworthy that the initial and the reference configurations are defined to be the undeformed state of the soft system, which is a hypothetical state that does not exist in reality because of the intrinsic magnetic force. This definition requires us to apply the mechanical and magnetic boundary conditions to the system simultaneously. The advantages of the decoupled approach are twofold. First, the initial configuration can be used to evolve the system to calculate the magnetic flux density and magnetic field of the system. In this way, the calculation of the magnetic field and magnetic flux density can be eliminated in the reference configuration (fig. S2). Such a methodology will be particularly advantageous in scenarios

where the relationship between $\vec{m}$ and $\vec{M}$ is complex, and the formulation of the magnetic constitutive relationship is a challenge in the reference configuration. Second, this approach accentuates that the magnetoelastic effect refers to the transformation of magnetic flux density and magnetic field from the initial configuration to the current one. This distinction helps to mitigate potential misunderstandings that the magnetoelastic effect pertains to a transformation between the reference and current configurations.

The transformation of magnetization from the initial to the current configurations, describing the MC of soft systems, is intrinsically dependent on the material specifics within the system, rendering it fundamentally indeterminate, which can be written as

$$\vec{m} = f(\boldsymbol{F})\vec{M} \tag{1}$$

where $f(\boldsymbol{F})$ refers to a function of deformation gradient $\boldsymbol{F}$ and satisfies $f = \boldsymbol{I} \,@\, \boldsymbol{F} = \boldsymbol{I}$. For our system of interest, an appropriate assumption is depicted below

$$\vec{m} = \boldsymbol{R}\vec{M} \tag{2}$$

where $\boldsymbol{R}$ is the rotation matrix in the polar decomposition of $\boldsymbol{F}$. This assumption is reasonable because (i) the soft system of interest can be considered as an ideal soft magnetoelastic system whose magnetization should be insensitive to the pure stretch (note S1). (ii) Magnetization can be considered as a vectorial quantity associated with the density of the material in the reference and current configuration. For incompressible materials whose density did not change with deformation, the magnetization will only change its direction according to the rotation matrix of the deformation but maintain its magnitude as a constant. (iii) The intrinsic magnetoelastic effect of magnetic particles should be minimal in the stress range of 100 kPa. (iv) The simulation in the microscopic scale supports the proposed assumption (note S2). (v) The rotation of materials in soft magnetoelastic systems is analogous to the rotation of the magnetic domain in rigid metals and metal alloys. (vi) It has been validated in the simulation of the magnetic-to-mechanical response of soft systems, aligning with the corresponding experimental results (*33*, *37*).

Equation 2 and Fig. 1B exemplify our central hypothesis on the principal genesis of the magnetoelastic effect in isolated permanent magnetic soft systems: the rotation of material magnetization coupling with the pronounced nonlinear geometry variation, as schemed in Fig. 1C.

Constitutive equations

We consider the giant magnetoelastic effect as the result of magnetic field variation under a finite deformation of the soft magnetoelastic system from the initial to the current configuration. The mechanical part of the soft magnetoelastic system is solved in the reference configuration. The equilibrium equation governing the mechanical behavior of the system in the reference configuration can be written below

$$\nabla \cdot \boldsymbol{F}\boldsymbol{S} = 0 \tag{3}$$

where $\boldsymbol{S}$ have the contributions from both the mechanical and magnetic parts and can be written as the function of the system's free energy density $W\left(\boldsymbol{F}, \overrightarrow{M_r}, \overrightarrow{H_r}\right)$ as below

$$\boldsymbol{S} = 2\frac{\partial W\left(\boldsymbol{F}, \overrightarrow{M_\mathrm{r}}, \overrightarrow{H_\mathrm{r}}\right)}{\partial \boldsymbol{C}} \tag{4}$$

Here, $W\left(\boldsymbol{F}, \overrightarrow{M_\mathrm{r}}, \overrightarrow{H_\mathrm{r}}\right)$ is composed of the mechanical and magnetic parts as below (*37*)

$$W\left(\boldsymbol{F}, \overrightarrow{M_\mathrm{r}}, \overrightarrow{H_\mathrm{r}}\right) = \frac{G}{2}\left(I_1 - 3\right) - \frac{1}{2}\mu_0\overrightarrow{H_\mathrm{r}} \cdot \boldsymbol{C}^{-1}\overrightarrow{H_r} - \mu_0\overrightarrow{M_\mathrm{r}} \cdot \boldsymbol{C}^{-1/2}\overrightarrow{H_\mathrm{r}} \tag{5}$$

where G is the shear modulus of the Neo-Hookean material, I_1 is the first invariant, and μ_0 is the vacuum permeability. More details are explained in note S3. By writing the free energy density as a function of $\boldsymbol{C}$, the symmetry of the total Cauchy stress tensor and the balance of angular momentum are automatically satisfied.

The magnetic properties of the soft magnetoelastic system are calculated using the evolution of the initial configuration and are governed by Maxwell's equations in their differential forms. When the initial configuration evolves to the current configuration, excluding consideration of the electrodynamic effect and electric current, the equations can be written as below

$$\nabla \cdot \vec{b} = 0 \tag{6}$$

$$\nabla \times \vec{h} = 0 \tag{7}$$

The relationship between $\vec{b}$, $\vec{h}$, and $\vec{m}$ is governed by the constitutive equation

$$\vec{b} = \mu_0\left(\vec{h} + \vec{m}\right) \tag{8}$$

where μ_0 is the vacuum permeability. With Eq. 2, the constitutive equation transfers to

$$\vec{b} = \mu_0\left(\vec{h} + \boldsymbol{R}\vec{M}\right) \tag{9}$$

$\boldsymbol{R}$ is obtained by solving the deformation using the reference configuration.

Boundary conditions

The boundary conditions of the theoretical framework can be separated into the magnetic and mechanical parts. When the initial configuration evolves to the current configuration, the boundary conditions of the magnetic part, excluding consideration of surface current, can be written as

$$\left(\overrightarrow{b_\mathrm{o}} - \overrightarrow{b_\mathrm{i}}\right) \cdot \vec{n} = 0 \tag{10}$$

$$\left(\overrightarrow{h_\mathrm{o}} - \overrightarrow{h_\mathrm{i}}\right) \times \vec{n} = 0 \tag{11}$$

where $\overrightarrow{b_\mathrm{o}}$ and $\overrightarrow{b_\mathrm{i}}$ are the magnetic flux densities on the outside and inside of the boundary, respectively; $\overrightarrow{h_\mathrm{o}}$ and $\overrightarrow{h_\mathrm{i}}$ are the magnetic fields on the outside and inside of the boundary, respectively.

The boundary condition of the mechanical part in the reference configuration can be separated into two parts. The first part is the Maxwell stress as surface traction applied to the deformable solid (*38*), which can be expressed as

$$F_\mathrm{mag} = \int_{\partial V} \boldsymbol{t_o}\vec{n}\, ds = \int_{\partial V}\left[\frac{1}{\mu_0}\overrightarrow{b_\mathrm{o}} \otimes \overrightarrow{b_\mathrm{o}} - \frac{1}{2\mu_0}\left(\overrightarrow{b_\mathrm{o}} \cdot \overrightarrow{b_\mathrm{o}}\right)\boldsymbol{I}\right]\vec{n}\, ds \tag{12}$$

The $\overrightarrow{b_o}$ is obtained using the evolution of the initial configuration. This Maxwell surface traction arises from the contribution of magnetic energy outside the materials (*19*, *38*, *39*). Equation 12 is defined in the current configuration but can be transformed to the reference configuration as below (*38*)

$$\boldsymbol{T_o} = \boldsymbol{t_o F}^{-T} \tag{13}$$

The second part of the mechanical boundary condition is determined by the different deformation modes from stretch, twist, and shear to local deformation, compress, and bend (Fig. 1D) through implementing different kinematic constraints on the boundary conditions. For instance, boundary conditions of the shear deformation can be expressed as

$$\overrightarrow{x_t} = \overrightarrow{X_t} + \Delta\, \mathrm{d}\, \vec{\mathrm{i}} \tag{14}$$

$$\overrightarrow{x_b} = \overrightarrow{X_b} \tag{15}$$

where $\overrightarrow{x_t}$ and $\overrightarrow{X_t}$ represent the coordinates of the top surface in the current configuration and reference configuration; $\overrightarrow{x_b}$ and $\overrightarrow{X_b}$ represent the coordinates of the bottom surface in the current configuration and reference configuration; $\Delta\, \mathrm{d}\, \vec{\mathrm{i}}$ indicates the shear distance of the top surface from the reference configuration to the current configuration in the X direction. Other deformation modes of the soft magnetoelastic system can be elucidated analogously to the shear deformation approach.

The aforementioned equations facilitate the separation of calculations related to the mechanical and magnetic components of the soft system into two distinct configurations. An alternative methodology, which concurrently solves both mechanical and magnetic components within the reference configuration, is elaborated upon in note S4. These two approaches yield the same results. The calculation using two distinct configurations will be implemented into the following finite element implementation and result analysis.

Finite element implementation

The developed theoretical framework is seamlessly integrated into the COMSOL finite element environment. The arbitrary Lagrangian-Eulerian method is applied to account for the interface movement during deformations (note S5). Before implementation, it is imperative to experimentally ascertain the initial magnetization M and the shear modulus G of the soft magnetoelastic system, respectively. The initial magnetization M is determined by measuring the magnetic flux density B_z of the sample with both cylinder and cuboid geometries. The rationale for using samples of two distinct shapes is to facilitate an investigation into potential shape-induced effects. As displayed in Fig. 1E, B_z of the soft magnetoelastic system is linearly proportional to the volume fraction of the micromagnets and can be expressed as

$$B_z = kc_p \tag{16}$$

where k is a constant representing the magnetic flux density of micromagnets and c_p is the particle volume concentration. Notably, the sample's geometry exerts only a marginal influence on its magnetic flux density. This observation aligns with expectations, given that the surface area and height of the samples, irrespective of their geometric form, were meticulously maintained to be consistent. Unlike magnetic flux density, the shear modulus of the soft magnetoelastic system demonstrates a nonlinear increase with respect to the particle volume concentration (Fig. 1F). Specifically, the shear modulus exhibits a pronounced acceleration in its increase when the particle volume concentration exceeds 10%. The nonlinear correlation between shear modulus and particle volume concentration can be predicted using the Mooney model (*34*, *40*). This model, adapted from the Einstein equation, posits that the increase in modulus in a composite system is analogous to the rise in viscosity in a suspension, considering interparticle interactions

$$G = G_0 \exp\left(\frac{2.5c_p}{1 - Sc_p}\right) \tag{17}$$

where G_0 denotes the shear modulus of the pure elastomer without particles. S is the crowding factor, and an optimal value of 1.25 provides the closest fit to the experimental results. By integrating the experimentally obtained values of M and G into the theoretical framework and the finite element environment, the giant magnetoelastic effect can be analyzed in soft systems across arbitrary geometries, deformation modalities, and magnetization profiles.

Compression deformation

Before comparing the results garnered from the theoretical framework with experimental data, we initially ascertain the accuracy of the proposed model by contrasting it with the analytical solution for a cylindrical soft magnetoelastic system subjected to biaxial stretching (Fig. 2A). During this evaluative process, the incorporation of magnetic force into the model is deliberately omitted, as its inclusion precludes the derivation of an analytical solution. This analytical solution can be obtained by solving Maxwell's equations using Green's function (note S6). Figure 2B shows the Z-directional magnetic flux density (b_z) at the top surface center under various biaxial stretching conditions, while Fig. 2C presents b_z at the body center, comparing the modeling and analytical results. The modeling results align well with the analytical solution, confirming the accuracy of the proposed theoretical framework. Additional observations reveal that b_z decreases linearly when the system undergoes biaxial stretch. However, a nonlinear behavior is identifiable when the magnitude of the stretch intensifies. Taking a step further, b_z along the vertical axis of the soft magnetoelastic system under various biaxial stretching conditions is depicted in Fig. 2D. Observably, there is a decrement in the Z-directional magnetic flux density as biaxial stretching progresses. Notably, the modeling outcomes are in congruence with the analytical solution across the entire spectrum of conditions. These findings not only bolster the validity of the model but also enhance the confidence in comparing the modeling results with experimental data under more complex deformation scenarios.

After validating the model under biaxial stretch conditions, the theoretical framework is subsequently used to simulate the giant magnetoelastic effect in the cylindrical system under practical compression (Fig. 2E). Figure 2F presents the obtained simulation results of b_z on the top surface and vertical cross sections of the system, both in its initial state and after being compressed to 86% of its original height. Figure S3 further illustrates the bulk b_z and the direction of magnetic flux, which follows the rotation matrix defined in Eq. 2. Both results reveal a decrease of b_z in the soft magnetoelastic system under compression deformation, showing the same trend as the previously reported giant magnetoelastic effect in soft systems (*7*). To quantify the precision of the proposed theoretical framework, the correlation between b_z and applied stress was further simulated

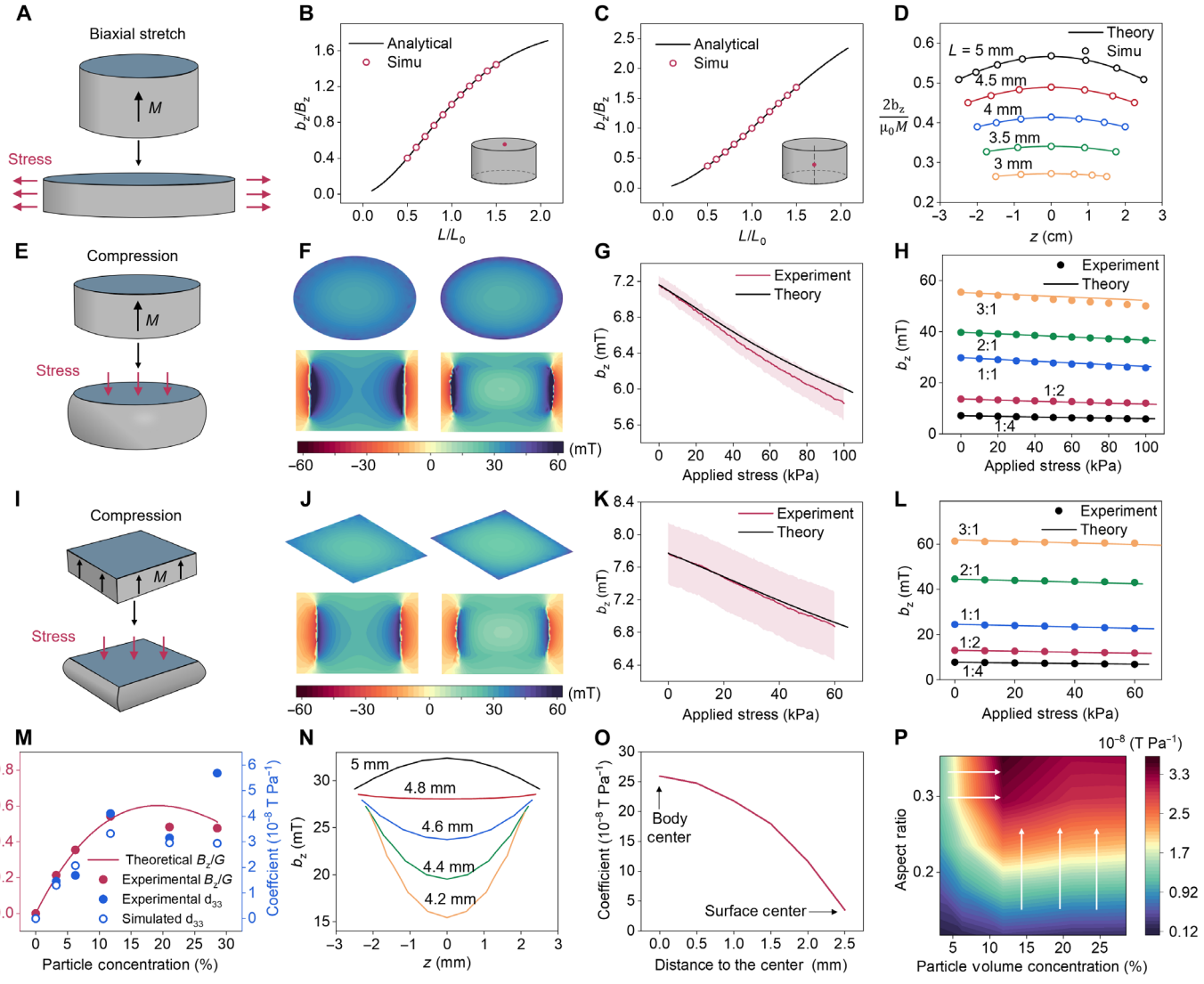

Fig. 2. Investigate the magnetoelastic effect in soft systems with a compression deformation mode. (**A**) Scheme of a cylindrical magnetoelastic system subject to biaxial stretch. (**B** and **C**) Simulation (Simu) result and analytical solution are consistent for the b_z at both the surface center (B) and the body center (C) under the biaxial stretch. $L_0 = 5$ mm. (**D**) Normalized b_z along the axis of the cylindrical system under various biaxial stretching conditions. (**E**) Scheme of a cylindrical magnetoelastic system subject to compression. (**F**) Simulated b_z mapping on the top surface and cross section of the cylindrical system in its initial and compressed states. (**G** and **H**) Relationship between b_z and applied stress at the surface center of the cylindrical system with different micromagnet-to-polymer weight ratios includes 1:4 (G) and the summary (H). Experimental results represent the average value from three independent experiments. Shaded area represents the SD. (**I**) Scheme of a cuboidal magnetoelastic system subject to compression. (**J**) Simulated magnetic flux density mapping on the top surface and cross section of the cuboidal system in its initial and compressed states. (**K** and **L**) Relationship between b_z and applied stress at the surface center of the cuboidal system with different micromagnet-to-polymer weight ratios includes 1:4 (K) and the summary (L). Experimental results represent the average value from three independent experiments. Shaded area represents the SD. (**M**) Prediction of the variation of B_z/G, a quantity that characterizes the MC factor, with the particle volume concentration for the cylindrical system. (**N**) b_z along the cylindrical axis when the system is compressed from 5 to 4.2 mm. (**O**) The simulated MC factors at distinct positions inside the cylindrical system. (**P**) Mapping of MC factor with respect to the particle volume concentration and the aspect ratio predicted by the model.

and compared to the experimental result. For a comprehensive analysis, we conduct both simulations and experiments across five soft magnetoelastic systems with micromagnet-to-polymer weight ratios ranges of 1:4, 1:2, 1:1, 2:1, and 3:1. The corresponding results are shown in Fig. 2 (G and H) and fig. S4. It is evident that the simulation results align closely with experimental observations. Such exceptional consistency between simulations and experiments across systems with diverse compositions underscores the robustness and reliability of the proposed theoretical framework. It further suggests that the underlying assumptions of the theoretical framework aptly capture the fundamental principles of MC physics in soft systems.

To investigate the impact of system geometry on the magnetoelastic effect and determine whether the theoretical framework captures this influence, parallel simulations and experiments were conducted on a cuboidal system, whose top surface area and height

are equated to those of the cylindrical counterpart (Fig. 2I). Figure 2J presents the obtained simulation results of b_z on the top surface and vertical cross sections of the cuboidal system, both in its initial state and after being compressed to 86% of its original height. Meanwhile, the bulk b_z and the direction of magnetic flux are displayed in fig. S5. Similar to the cylindrical system, decreasing b_z under compression deformation is observed. Comparing the simulated b_z-applied stress curves with experimental data for the cuboidal system, as illustrated in Fig. 2 (K and L) and fig. S6, yields conclusions akin to those for the cylindrical system: The simulation aligns closely with experimental observations. Such results robustly affirm that system geometry exerts minimal impact on the model's accuracy, underscoring the universality of the proposed theoretical framework.

Upon analysis of the b_z-applied stress curves, we can subsequently derive the MC factor, denoted as d_{33}. Figure 2M and fig. S7 compare the experimental and simulated d_{33} obtained in the cylindrical and cuboidal systems, respectively, with different particle volume concentrations. Besides the anticipated agreement between simulated and experimental d_{33} values, a noteworthy observation is the nonlinear and nonmonotonic variation of d_{33} as a function of particle volume concentration in both systems. This complex d_{33} behavior can be understood from the nonsynergic increase of the reference magnetic flux density B_z and G with the particle volume concentration in the system. While B_z increases linearly, G shows exponential growth with the increase of the particle volume concentration and is further influenced by the magnetic force of the system. A higher B_z directly leads to a higher d_{33}, while a greater G indicates a reduced system deformation tendency, resulting in a lower d_{33}. Thus, an intuitive scaling parameter B_z/G can be proposed and proven to capture the trend of d_{33}, as evidenced by Fig. 2M. It is worth noting that B_z/G intrinsically links the magnetic and mechanical properties of soft systems and shares the same unit with d_{33}. Therefore, it serves as an appropriate metric to elucidate the magnetoelastic coupling characteristics of soft systems. A detailed discussion of the relationship between B_z/G and d_{33} is further presented in note S7.

The most crucial characteristic of a physical model is its predictability. Having demonstrated its consistency with experimental results in both cylindrical and cuboidal systems undergoing compression deformation, we aim to leverage this established model to delve deeper into the characteristics and underlying principles of the giant magnetoelastic effect in a generalized soft magnetoelastic system subjected to compression deformation. Our specific goal is to use this model to forecast magnetoelastic behaviors that have not yet been observed in experiments. The first insight obtained from the model is that the magnetoelastic behavior in the soft system is position dependent. As displayed in Fig. 2N, the b_z curve along the cylindrical axis exhibits a transformation from concave to convex during compression deformation. This indicates that the variation of b_z is more pronounced at the body center than at the bottom and top surface centers, as corroborated by the derived MC factor presented in Fig. 2O. Numerically, the predicted MC factor increases nonlinearly from 3.6×10^{-8} T Pa^{-1} at the top surface center to 2.6×10^{-7} T Pa^{-1} at the body center. Notably, the factor at the body center is threefold the maximum recorded value observed on the surface to date (*7*). The model thus uncovers a previously unobserved characteristic of the giant magnetoelastic effect in soft systems: The MC is most potent at the body center and progressively diminishes toward the surface in soft systems. Taking a step further, the volume-averaged b_z-applied stress curve is also calculated. As illustrated in fig. S8, the volume-averaged b_z-applied stress curve exhibits a steeper slope compared to the surface b_z-applied stress curve. A more detailed calculation reveals that the volume-averaged coupling factor is 5.5×10^{-8} T Pa^{-1}, approximately 4.17 times of the corresponding factor on the surface. This highlights the giant feature of the magnetoelastic effect in soft systems. The second insight of the theoretical framework arises from the simulation-derived d_{33} mapping with respect to the geometry of the system and the particle volume concentration as displayed in Fig. 2P. In addition to the correlation with particle volume concentration as expressed by B_z/G, which has been confirmed by experiments, the mapping further reveals an upward trend in d_{33} with respect to the aspect ratio of the cylindrical system throughout the entire particle volume concentration range. This anticipated behavior is further confirmed by additional experiments on a cylindrical system with an aspect ratio of 0.118, as demonstrated in fig. S9. This affirms the effectiveness and prediction capability of the theoretical framework. It is also noteworthy that the discoveries obtained from the cylindrical system are similarly observed in simulations of the cuboidal system, as evidenced in fig. S10. The theory has also been applied to systems with higher aspect ratios, and the results are displayed in fig. S11. Intuitively, the theory predicts that the b_z-compress displacement curve transitions from a linear to a parabolic decrease, with the slope diminishing as the system's aspect ratio increases. As the aspect ratio continues to increase, the theory further predicts that the magnetoelastic response shifts from negative to nonmonotonic, as illustrated in fig. S11 (C and F).

Examining the universality of the theoretical framework

Soft magnetoelastic systems under localized compression

After showcasing the accuracy and prediction capability of the theoretical framework for soft magnetoelastic systems under compression deformation, we took a further step to validate the universality of the theoretical framework by verifying its applicability across soft magnetoelastic systems subjected to various deformation modes, diverse magnetization profiles, and different architectures. Figure 3A displays the scheme of a cylindrical system subjected to localized compression. Here, the force is applied to a specific circular area with a radius of 2.1 mm. The corresponding simulated b_z versus applied stress curve is displayed and compared to the experimental results in Fig. 3B. The observed consistency between simulations and experiments suggests that the theoretical framework is pertinent and accurate for soft systems subjected to local compression. It is worth noting that the experimental data reveal a magnetic pole reversal phenomenon when the applied force exceeds 4 N. However, the simulation ceased at ~2.5 N due to substantial distortions in certain local meshes. To elucidate the experimentally observed magnetic pole reversal, the simulated b_z distribution at the top surface and the cross section of the system is depicted in Fig. 3C. Meanwhile, fig. S12 illustrates the bulk b_z, accompanied by the shape deformation, and the direction of magnetic flux in the cross-sectional b_z mapping. These visuals reveal that the periphery of the compressed area displays the same magnetic pole reversal phenomenon observed experimentally. Figure S13 further confirms that such a phenomenon can be attributed to the substantial rotation of magnetic materials in the rim region. These results lead to two important conclusions. First, the simulated b_z value of 12.75 mT at 2.5 N is a result of averaging the values across the entire compressed area. Thus, the

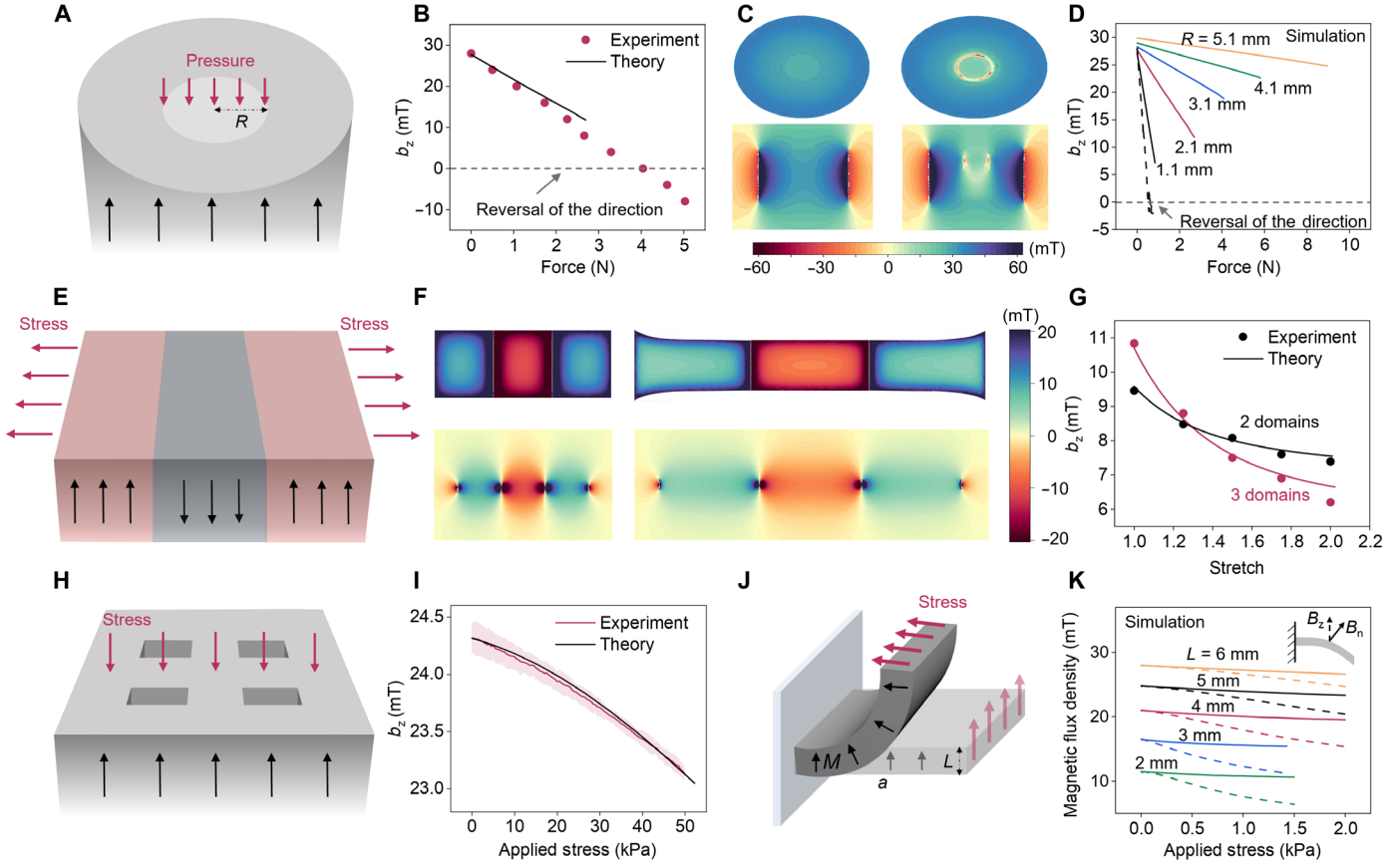

Fig. 3. Validate the universality of the framework for understanding the giant magnetoelastic effect in soft systems. (**A**) Scheme of a cylindrical system subjected to localized compression. (**B**) Comparison of the experimental and simulation b_z-force relationship under local compression. (**C**) Corresponding simulated b_z mapping on the top surface and cross section of the cylindrical system in its initial and compressed states. (**D**) Simulated b_z-force relationship under various local compression conditions, with the radius of deformation area ranging from 1.1 to 5.1 mm. Dashed line represents the modeling results not incorporating the magnetic force. (**E**) Scheme of a cuboidal system with three alternating magnetization domains subjected to uniaxial stretch. (**F**) Corresponding simulated B_z mapping on the top surface and cross section of the cuboidal system in its initial and stretched states. (**G**) Comparison of the experiential and simulated B_z-stretch curves for cuboidal systems with two and three magnetization domains. (**H**) Scheme of a soft lattice-structured magnetoelastic system subjected to compression. (**I**) Comparison of the simulated and experimental b_z-applied stress curves at the surface center of the lattice structure. Experimental results represent the average value from three independent experiments. Shaded area represents the SD. (**J**) Scheme of a cuboidal system subjected to bending deformation. (**K**) Simulated relationship between magnetic flux density and applied stress in the bent cuboidal system, with the thickness of the system varying from 2 to 6 mm. Solid lines depict the variation of b_n, while dashed lines indicate the variation of b_z.

simulation accurately reflects magnetoelastic principles in soft systems under localized compression and, absent mesh distortions, is projected to concur with experimental outcomes beyond 2.5 N. Second, considering that the magnetic material rotation predominantly occurs in the marginal region of the compression domain, it is anticipated that a reduced compression area would amplify the magnetic pole reversal phenomenon at lower forces. Simulation results of local compression with different radii of compression area in Fig. 3D strongly support this conclusion. When the radius of the compression area is reduced to 1.1 mm, the magnetic pole reversal can be simulated at only 0.6 N when the magnetic force is not incorporated in the model.

In addition to the magnetic pole reversal phenomenon, the theoretical framework elucidates two features in soft magnetoelastic systems under localized compression. First, the magnetoelastic effect is inversely correlated to the compression area. Not only that this feature is reflected by the slopes of b_z-applied force curves in Fig. 3D, but it is further validated by the magnetic flux variation of systems with different compression areas, as demonstrated in fig. S14. Second, the magnetoelastic effect in localized compression is stronger than in whole-body compression, evidenced by the difference in the magnetic flux density variation under both equivalent displacements (e.g., 13.3 versus 2.4 mT at 0.8 mm) and applied forces (e.g., 9.2 versus 0.22 mT at 1.5 N). This phenomenon can be elucidated from two points. First, rotational deformation of magnetic materials reduces b_z more effectively compared to pure compressive deformation. Second, localized compression encompasses a more substantial proportion of rotational deformation than whole-body compression, particularly in periphery areas. In essence, the theoretical framework has been proven to provide accurate results to the soft systems subjected to localized deformation modes (i.e., localized compression) and capture the underlying magnetoelastic principle. Together with the experiments, it has unveiled the magnetoelastic pole reversal, a unique phenomenon in soft systems and previously not reported in rigid metals and metal alloys, illuminating its underlying mechanism.

Magnetoelastic effect in soft systems with patterned magnetization profiles

Subsequent to establishing the adaptability of the theoretical framework across a multitude of deformation modalities, we extend its utility to soft systems characterized by patterned magnetization profiles. Specifically, we scrutinize the simulation results of soft cuboids that exhibit alternating magnetizations in the Z direction, subjected to uniaxial stretching, as schemed in Fig. 3E. Figure S15 and Fig. 3F showcase the simulation outcomes of two soft cuboids: one with two magnetization domains and the other with three. Comparing it to the experimental results in Fig. 3G reveals that the simulations yield a reduction in magnetic flux density, consistent with practical situations in both instances. This confirms the universality of the theoretical framework in accommodating systems with patterned magnetization domains. It is important to mention that b_z does not decrease linearly with the stretch. Alternatively, the decrement of b_z exhibits a progressively attenuated rate in response to continued stretching. This observation reiterates that a soft system can exhibit different magnetoelastic behaviors under different deformation modes. In addition, the decrease of b_z in the system with three magnetization domains surpasses that in the system with two magnetization domains. This trend can be attributed to the larger aspect ratio of each domain in the system with three magnetization domains.

Magnetoelastic effect in soft architectured systems

The theoretical framework can also be applied to soft architectured systems whose structure, dimension, and micro–computed tomography (micro-CT) are displayed in fig. S16. As schemed in Fig. 3H, parallel experiments and simulations are performed on a soft cuboidal system with a square lattice structure. Figure 3I displays the variation of b_z at the surface center of the system under compressive stress obtained from both the experiments and the simulations, with detailed results presented in fig. S17. It is evident that the simulation closely aligns with the experimental results, reaffirming the robustness and universality of the theoretical framework. Moreover, a meticulous analysis of the b_z-applied stress curves discerns an increasing rate of b_z attenuation in both experiments and simulations. Such an observation starkly contrasts with the behavior exhibited by unstructured soft systems, thereby dictating the unique magnetoelastic characteristics of architectured systems. Another observation is the increase of b_z within the voids of the lattice structure (fig. S17, F and G) despite the concomitant diminution of b_z in the surrounding magnetoelastic materials. One conceivable hypothesis posits that the overarching contraction of the voids amid compression deformation culminates in the intensification of magnetic flux lines. Yet, a more exhaustive exploration is imperative to provide a holistic elucidation of this observed phenomenon. Nevertheless, the accuracy, universality, and robustness of the theoretical framework are further strengthened through the investigation of soft magnetoelastic architectured systems.

Magnetoelastic effect in soft systems under bending and shearing deformations

After validating the universality of the model in soft magnetoelastic systems subjected to various deformation modes, diverse magnetization profiles, and different architectures, we aim to fully harness the underlying potential of the theoretical framework by conducting bending and shearing simulations to the soft magnetoelastic systems. In this way, major deformation modes will be covered to enable a more generalized insight into the magnetoelastic effect in soft systems. Figure 3 (J and K) and fig. S18 display the scheme of a soft bent cuboid along with its corresponding simulation results. In contrast to the compression and stretch deformation modalities, the bending deformation leads to a pronounced alteration in the orientation of the surface. Consequently, using b_z as a parameter to characterize the magnetoelastic effect is not apt in this context (fig. S18, A to D). A more fitting parameter is the normalized component b_n, which can be calculated through $\vec{b} \cdot \vec{n}$ and effectively represents the bending-induced magnetic flux variation. On the basis of the results from computational simulations, three salient features pertaining to the magnetoelastic effect in soft systems under bending deformation can be delineated. First, to achieve analogous magnetic flux density variations on the surface, the required applied stress is substantially reduced in comparison to the compression and stretch modalities, as illustrated in Fig. 3K. Second, the MC factor of the soft system under bending deformation demonstrates a nonmonotonic correlation with the height of the system, as illustrated in fig. S19A. Third, the bending modality manifests an asymmetric position dependence on the magnetoelastic effect, as corroborated by fig. S19B, in contrast to the compression situation. After the bending simulation, a shearing deformation simulation is performed on the soft cuboidal system, and the results are displayed in fig. S20. It can be seen that b_z decreases with increasing shear stress. In addition, the magnetoelastic effect caused by shear deformation demonstrates a positive correlation with the system height. A primary difference between shearing modality to other deformation modes is the amplified significance of whole system rotation in dictating the overall magnetoelastic effect, as confirmed in fig. S20D. To further elucidate the influence of whole system rotation on the magnetoelastic effect in the context of shearing modality, the relationship of Z-direction magnetization with respect to applied shear stress is calculated and displayed in fig. S21. It is intriguing to observe that m_z/M_z is almost identical to b_z/B_z. This implies that the decrease of b_z in the system predominately results from the rotation of materials. This distinctive feature of shearing modality highlights the diversity of the magnetoelastic effect in soft systems arising from the different deformation modes.

Magnetoelastic effect in soft systems with different initial magnetization directions

In previous discussions, the initial magnetization direction was constrained to the z axis. However, magnetization is a vector quantity that can assume any arbitrary direction. To evaluate the impact of initial magnetization direction on the magnetoelastic effect, additional calculations were conducted on the cuboidal systems. As depicted in fig. S22A, simulations were conducted for various scenarios in which the initial magnetization was varied from the positive Z direction to a 45° deviation from the positive z axis. The corresponding cross-sectional b_z mapping, along with the mapping of magnetic flux density directions, is displayed in fig. S22B. It is observed that for systems with initial magnetization directions not aligned with the positive z axis, the application of compression substantially alters the orientation of the magnetic flux density, particularly within the deformable systems. However, the variation in the surface Z-direction magnetic flux density is highest when the initial magnetization is in the positive Z direction, evidenced by both the b_z-compress distance curves in fig. S22C and the corresponding coupling factor in fig. S22D. This phenomenon occurs because when the initial magnetization deviates from the positive Z direction, its Z-direction component decreases due to the conservation of the total magnetization amplitude. The results indicate a direct correlation

between MC in a given direction and the magnetic field along that axis. Consequently, to maximize the coupling factor in a particular direction, the initial magnetization should be optimally aligned with that direction.

Overall, the versatility of the theoretical framework to capture the vast spectrum of magnetoelastic phenomena across a range of soft systems has been validated. Through meticulous simulations, we elucidate the vast array of magnetoelastic effects inherent to various soft systems. This achievement lays a firm foundation for the in-depth understanding and practical applications of the giant magnetoelastic effect in soft systems.

Technological impact of the framework

To showcase the technological impact of the theoretic framework for the giant magnetoelastic effect in soft systems, we took a further step to use a deformable soft coil to convert the pressure-induced magnetic field variation in the soft magnetoelastic materials into electricity and invented an all-in-one soft MEG for mechanical pressure to electricity conversion, as depicted in Fig. 4A. Technically, the soft magnetoelastic materials act as the MC layer to transform mechanical perturbations into distinctive variations of magnetic flux density. Subsequently, the coil operates as the MI layer to convert the variation of magnetic flux density into useful electrical signals. In this way, the soft MEG emerges as a new platform technology for mechanical-to-electrical conversion with a wide range of applicability from energy, and sensing, to therapeutics. To elucidate the electrical output of soft MEG using diverse magnetoelastic materials under assorted deformation modes, a general theory is developed by integrating the theoretical framework for the magnetoelastic effect of the MC layer and Faraday's law for the MI layer (note S8). This integration yields the following equation (*41*, *42*)

$$\varepsilon_t = -\sum_{i=1}^{n}\left\{\iint_{S(t)}\frac{\partial \vec{b}\left(\vec{r},t\right)}{\partial t}\cdot d\overrightarrow{A_i} - \oint_{\partial S(t)}\left[\vec{v}\times\vec{b}\left(\vec{r},t\right)\right]\cdot d\vec{l}\right\} \quad (18)$$

where ε_t represents the voltage output of the soft MEG, n represents the number of coil turns in the MI layer, $S(t)$ represents the time-varied integration area in the MI layer, $\vec{b}\left(\vec{r},t\right)$ denotes the magnetic flux density perceived by the MI layer, and $\vec{v}$ represents the instantaneous velocity of the movement of every line element in $\partial S(t)$ at time t. Equation 18 elucidates that the voltage generated by soft MEGs comprises two salient components. The first term epitomizes the contribution ascribed to the magnetoelastic effect inherent to the MC layer. In juxtaposition, the second term describes the voltage generation due to the deformation of the MI layer, resulting from an intersection of the coil with the magnetic field. Within the context of the established theoretical framework addressing the magnetoelastic effect in the MC layer, the precise determination of $\vec{b}\left(\vec{r},t\right)$ becomes achievable. Thus, upon specifying $\vec{v}$, the entirety of the electrical output for the soft MEG can be determined by Eq. 18. Correspondingly, the short-circuit current I_{sc} of soft MEGs can be derived in the low-frequency range as

$$I_{sc} = -\sum_{i=1}^{n}\left\{\iint_{S(t)}\frac{\partial \vec{b}\left(\vec{r},t\right)}{R\,\partial t}\cdot d\overrightarrow{A_i} - \oint_{\partial S(t)}\frac{\left[\vec{v}\times\vec{b}\left(\vec{r},t\right)\right]}{R}\cdot d\vec{l}\right\} \quad (19)$$

where R represents the internal resistance of the MI layer. When applying Eqs. 18 and 19 to various deformation modes of soft MEGs, a classification of deformation modes (Fig. 4B) arises naturally based on whether the deformation of MI layers is restricted to mere translational movement (type 1) or encompasses additional deformative characteristics (type 2). For deformation modes categorized as type 1, where the MI layer experiences strictly translational movement (e.g., shearing and compression), it can be substantiated that the electrical output of the soft MEG is exclusively correlated with the alterations in magnetic flux density discerned by the MI layer (note S9). For deformation modes classified as type 2, which include bending, stretching, and local deformation, the contribution of motional voltage cannot be neglected, and each mode is associated with a specific analysis leading to distinctive voltage expressions detailed in note S10. Notably, the analysis reveals substantial motional voltage in stretching deformation, particularly in biaxial stretching. Nevertheless, it should be emphasized that the generated voltage arises from the magnetic flux variation perceived by the MI layer, regardless of the origin being motional or induced.

The developed theory of soft MEGs is poised for validation against empirical results to underscore its accuracy and tenacity. However, before this comparative assessment, it remains paramount to confirm the consistency between simulated magnetic flux variations and the analytical solutions. Analogous to the exploration of the magnetoelastic effect in soft systems, biaxial stretching deformation of a cylindrical configuration is chosen, because the analytical solution can be readily derived for this system (note S11). Figure 4C displays the comparison of simulated magnetic flux and the analytical results. First, the simulation outcomes align with the analytical solution, affirming the precision and resilience of the advanced theoretical framework for magnetic flux computation. Consequently, this framework ensures accurate magnetic flux values for subsequent electrical output estimations. Second, the total magnetic flux increases with increased stretching in the biaxial stretch deformation. Since the induced change of magnetic flux density contributes negatively to the total magnetic flux, this observation directly reveals that the motional voltage dominates the electrical output of the soft MEG under biaxial stretch deformation.

After validating the theoretical framework for magnetic flux calculation, the accuracy of the theory in soft MEGs is then evaluated using a practical cuboidal MEG under compression deformation. The particle-to-polymer weight ratio of the MC layer is assigned to be 1:1. The MI layer contains 90 turns of the coil in a plane with a linewidth of 76.2 μm, as shown in Fig. 4D and fig. S23. In the experimental setup, the soft MEG is subjected to a sinusoidal displacement. The range of this displacement, along with the simulated magnetic flux variation derived from the theory of the magnetoelastic effect, is illustrated in Fig. 4E. In accordance with the theoretical framework, the electrical output of the soft MEG under compression deformation can be approximated as the induced voltage resulting from magnetic flux variations within the MI layer. Figure 4 (F and G) displays the calculated and experimental results of the short-circuit current and open-circuit voltage of the soft MEG under compression, respectively. Both the current and voltage measurements manifest a commendable alignment between theoretical propositions and empirical results. In addition, the theoretical framework successfully captures the frequency dependence of the output of a soft MEG, with corroborative evidence provided for the 5-Hz scenario in fig. S24. Notably, both theoretical and experimental results display the asymmetric feature of the signal

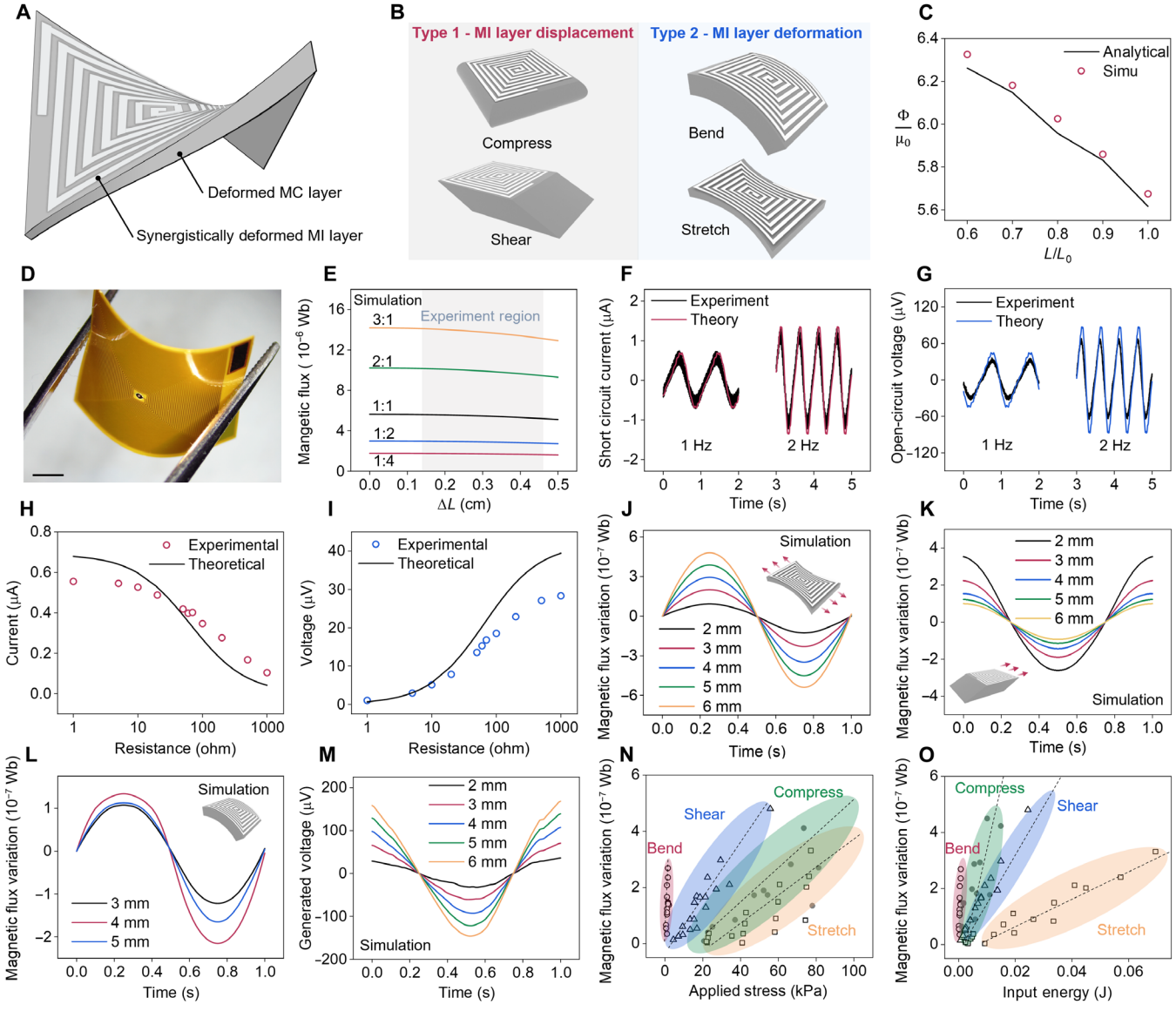

Fig. 4. Validate the theoretical framework by showcasing a soft MEG. (**A**) Scheme of a soft MEG with a deformed MC layer and a synergistically deformed MI layer. (**B**) The voltage expression of soft MEGs can be classified into two categories based on the deformation modes. Type 1 includes compression and shearing. Type 2 includes bending, stretching, and local deformation. (**C**) Comparison of simulated and analytically derived magnetic flux when the system is subjected to various biaxial stretching conditions. (**D**) Photograph of the flexible MI layer used in the validation experiments. Scale bar, 3 mm. (**E**) Simulated magnetic flux variation of cylindrical MEGs with different micromagnet concentrations under compression. $\triangle L$ is half of the compressed distance. The gray region indicates the range of sinusoidal compression exerted upon MEG in the experiment. (**F** and **G**) Short-circuit current (F) and open-circuit voltage (G) of the soft MEG under sinusoidal compression. (**H** and **I**) Peak current (H) and voltage (I) of the soft MEG with different external loads under 1-Hz sinusoidal compression. (**J** to **L**) Calculated variation of magnetic flux in cuboidal systems under diverse deformation modalities including stretching (J), shearing (K), and bending (L). (**M**) Calculated voltage of the cuboidal system under stretching. (**N**) Comparison of output capability and applied stress among different deformation modalities of soft MEG. (**O**) Comparison of output capability and input energy among different deformation modalities of soft MEG. The output capability is characterized by the magnetic flux variation.

outputs, indicating that the theoretically predicted nonlinear decrease of magnetic flux is in consonance with the practical manifestation. This observation provides convincing evidence to justify the robustness of both the theory of soft MEG and the theoretical framework for the magnetoelastic effect in soft systems. Taking a step further, the current, voltage, and power outputs of the soft MEG are obtained experimentally with different external loads from 1 to 1000 ohms. A comparison between the experimental measurement and the theoretical calculation is presented in Fig. 4 (H and I) and fig. S25. The same trend between theory and experiment can be observed across all three electrical parameters. The theoretical optimal resistance also matches the experimental data impeccably. These results reiterate the accuracy of both the theory concerning soft MEGs and the magnetoelastic effect in soft systems.

In addition, we apply the developed theory to evaluate the magnetic flux variation and the electrical output characteristics of the

cuboidal MEG. Predominantly, the investigation centered on the influence of deformation modality and the aspect ratio of the system. The variations in magnetic flux and the resulting open-circuit voltage for soft MEGs of various aspect ratios subjected to sinusoidal stretching, shearing, and bending are plotted in Fig. 4 (J to M) and fig. S26. First, the variation of magnetic flux falls within the range of 10^{-7} to 10^{-6} Wb, indicative of the determinative boundaries for the MEG's output potential. Second, the dependence of magnetic flux variation on the aspect ratio is determined by the deformation mode. In stretching, shearing, and bending, the magnetic flux variation shows positive, negative, and no correlation with the system's aspect ratio, respectively. This observation reemphasizes the diversity of magnetoelastic effects in soft systems. It is important to note that different deformation modalities are enabled by different forcing approaches such as the top surface displacement in the shearing deformation and the applied stress in the bending deformation (fig. S26). To directly compare the performance metrics of various deformation modalities in the soft MEG, the calculated magnetic flux variation, which characterizes the output capability, is uniformly plotted against the applied stress and input energy for different deformation modalities, as shown in Fig. 4 (N and O), respectively. These figures reveal that bending has the highest efficiency of mechanical-to-electrical conversion in terms of both applied stress and input energy among all four deformation modes. In contrast, stretching displays the lowest efficiency when accounting for both applied stress and input energy. Compressing and shearing each offer unique advantages. For instance, shearing can produce higher output when subjected to lower levels of applied stress. However, when evaluated in the context of input energy, compression manifests enhanced efficiency, a consequence directly attributable to fewer surface displacements. It warrants further emphasis that while bending manifests the pinnacle of efficiency, it concurrently presents a conspicuously lower upper conversion threshold compared to the other three deformation modalities. The above results highlight that each deformation mode has its specific domain of optimal performance, and the choice between them should be contingent upon the desired outcomes and constraints of a particular application.

Overall, the developed theoretical framework lays a firm foundation for understanding and optimizing the performance of soft MEGs. Through the analysis of the established theory, we identify the advantages and disadvantages of each deformation modality, paving the way to customize the future design of high-performance soft MEGs.

DISCUSSION

Having established comprehensive theoretical frameworks for the magnetoelastic effect in soft systems, we revisit the distinction between the traditional magnetoelastic effect in metal/metal alloys and the magnetoelastic effect in soft systems within the proposed theoretical paradigm. The traditional magnetoelastic effect can be summarized by the constitutive Eq. 20,

$$\vec{b} = \mu_0\left(\vec{h} + \vec{m}\right) = \mu_0\left[\vec{\mathrm{m}}(\sigma)\mathrm{k} + \vec{\mathrm{m}}(\sigma)\right] = \mu_0(1+k)\vec{m}(\sigma) \quad (20)$$

where σ is the applied stress and k is a constant, denoted as a demagnetization factor related to the geometry of the system. Because of the material brittleness, compression is the major approach to induce the magnetoelastic effect in metal/metal alloys. During the compression process, the geometric configuration persists nearly invariant in the system. Hence, magnetic flux density is a single function of magnetization, which, in turn, is contingent upon the applied stress. In stark contrast, the constitutive equation for the magnetoelastic effect in soft systems can be summarized in Eq. 21

$$\vec{b} = \mu_0\left(\vec{h} + \vec{m}\right) = \mu_0\left[\vec{\mathrm{m}}(\mathbf{R})\mathrm{k}(\mathbf{F}) + \vec{\mathrm{m}}(\mathbf{R})\right] = \mu_0\vec{m}(\boldsymbol{R})\left[1 + k(\boldsymbol{F})\right] \quad (21)$$

Different from the situation of rigid metal/metal alloys, soft systems can have large deformations. As a result, the demagnetization factor k is not a constant but a function of the deformation gradient matrix $\boldsymbol{F}$. In addition, the magnetization of the soft materials is a function of the rotation matrix $\boldsymbol{R}$. Thus, magnetic flux density in soft systems is a function of both the demagnetization factor and material magnetization. This dual dependence of magnetic flux density, together with the versatile deformability, gives rise to a key feature of the magnetoelastic effect in soft systems: diversity. A wide range of unique magnetoelastic phenomena, not present in rigid systems, can emerge in soft systems. For instance, soft systems exhibit various magnetoelastic deformation modalities, while rigid systems have only compression. Each modality in soft systems further displays unique magnetoelastic characteristics manifested as the distinctive relationship between magnetic flux density and applied stress (e.g., linear, concave, convex, and nonmonotonic); different position dependence behavior; different contribution from $\vec{m}(\boldsymbol{R})$ and $k(\boldsymbol{F})$; distinguishing aspect ratio dependence; and the peculiar magnetic pole reversal observed in local compression. A comprehensive summary of the magnetoelastic effect across different deformation modalities in soft systems is displayed in table S1.

A central concept of our theoretical framework is to define the magnetization transformation between undeformed and deformed states of the soft system. This concept helps elucidate the non-uniqueness of magnetic constitutive relationship in the Lagrangian form (*43*). Within the context of our theoretical framework, the non-uniqueness of the magnetic constitutive equation in the reference configuration is a consequence of using different magnetization transformations between the initial and current configurations. As a result, the MC and calculated magnetoelastic effects will be different. In other words, the non-uniqueness of the magnetic constitutive relationship in reference configuration is a direct result of disparate soft systems exhibiting distinct magnetoelastic behaviors. Note S12 discussed the outcomes derived from using various magnetization transformations within the theoretical framework. The analysis confirms that the application of the transformation $\vec{m} = \boldsymbol{R}\vec{M}$ produces the most precise alignment with experimental results.

One important feature of our proposed theoretical framework is that it is rooted in the fundamental constitutive equations, Maxwell's equations, and mechanical equilibrium equations with appropriate assumptions. Consequently, the framework is universally robust and accurate (i.e., validated through a set of experiments) across various soft magnetoelastic systems subjected to various deformation modes, different micromagnet concentrations, diverse magnetization profiles, and distinct geometric structures. As a result, several important features of the magnetoelastic effect in soft systems can be summarized and predicted. For example, a scaling parameter B_z/G can be sublimated from the theoretical framework. This experimentally obtainable parameter quantifies MC entirely for systems with varying micromagnet concentrations and a constant

geometry. In addition, the theory points out that the MC factor at the body center of a soft system can reach up to 2.6×10^{-7} T Pa^{-1}. This surpasses the highest experimentally reported values by threefold, underscoring the substantial and underexplored potential of the magnetoelastic effect in soft systems.

Our proposed theoretical framework is a macroscopic model focusing on the modeling of the magnetoelastic effect in soft systems with large deformability. In such systems, the magnetoelastic effect can be mainly attributed to the macroscopic deformation and the magnetization redistribution. On the other hand, micromechanical models are suitable for modeling rigid magnetoelastic composites whose magnetoelastic effect mainly arises from the domain reorientation inside the magnetic particles (*14*–*16*, *18*). Both our approach and the micromechanical approach are two equally important methodologies focusing on different aspects of the magnetoelastic effect in composite systems (note S13).

The impact of magnetic forces can be elucidated through a comparative analysis of simulation results that either incorporate or omit the magnetic contribution to the system's free energy. In summary, the influence of magnetic force on the behavior of an isolated permanent magnetic soft system can be understood from two key aspects. First, the magnetic force leads to an increase in the system's modulus, with the magnitude of this increase being positively correlated with particle concentration. Second, it induces self-deformation in the system, which is most pronounced in systems with specially designed geometries and magnetization distributions. A detailed analysis of these effects is provided in note S14. Nevertheless, for isolated permanent magnetic soft systems with regular geometry and low particle concentration, the magnetic force demonstrates a minimal influence on the simulation of the magnetoelastic effect. This can be ascribed to the relatively weak magnetic fields of soft systems incorporating hard magnets.

Besides the theoretical framework for the magnetoelastic effect in soft systems, we also propose and study the theory of soft MEGs. Commencing with a comprehensive theory designed to encompass a broad spectrum of deformations in soft MEGs across diverse device architectures, we subsequently undertake an in-depth investigation into four fundamental deformation modalities: compression, stretching, shearing, and bending. Our results highlighted that each modality has distinct strengths and limitations, as summarized in table S2. Together with the result of the magnetoelastic effects in soft systems, we can conclude four key points to optimize the design of high-performance MEG. First, localized deformation enhances magnetoelastic coupling efficiency, as it involves increased rotational deformation, which is more effective in altering the magnetic flux density. Second, the initial magnetization direction of the MC layer should be oriented perpendicular to the MI layer to maximize magnetic flux density variation. Third, when designing the structural MC layer, minimizing the effective modulus while maximizing the initial magnetic flux density should be a guiding principle to achieve optimal magnetoelastic coupling efficiency. Fourth, the aspect ratio and deformation modality are critical parameters that influence both the trend and magnitude of magnetic flux density variation and should be considered in MEG design.

Last, we should emphasize that although the model demonstrates adequate concordance in soft magnetoelastic systems, some deviations are observed for the systems of high micromagnet concentrations, particularly the 28.57 vol % system. The discrepancy observed in the model for systems with high micromagnet concentrations can be attributed to three aspects. First, the intrinsic magnetoelastic effect of magnetic particles may start to emerge. Second, the assumption that $\vec{m} = \boldsymbol{R}\vec{M}$ may have its limitations in systems with a micromagnet concentration of 28.57 vol %. In those systems, it is anticipated that a substantial portion of micromagnets may interconnect with one another and not be entirely encapsulated by the polymer matrix. On one hand, the close distance between micromagnets leads to a heightened perceived magnetic field for individual particles, undermining the validity of the ideal hard ferromagnetism assumption. On the other hand, the collision-induced magnetoelastic effect inside the particle is not considered in the current framework. Third, the isochoric assumption may not be valid in systems of high micromagnet concentrations due to the increased incidence of entrapped air bubbles inside the system. Therefore, there remains substantial merit in the exploration of a more sophisticated theory founded upon meticulously refined assumptions. A viable approach involves refining the magnetization transformation equation and the system's free energy, using the representation theory in macroscopic models (*19*, *22*) and the constitutive relationships developed in micromechanical models (*15*, *18*).

We have developed a theoretical framework to study the magnetoelastic effect in soft systems. The theory is proven to be universally accurate and robust across various soft magnetoelastic systems subjected to various deformation modes, different micromagnet concentrations, diverse magnetization profiles, and distinct geometric structures. Through analysis of the proposed theory, we show the diversity of the magnetoelastic effect in soft systems and uncover substantial new phenomena including the magnetic pole reversal and the record-breaking MC factor of 2.6×10^{-7} T Pa^{-1} at the body center of the system. To show its technological impact, we further develop a general theory of soft MEGs capable of elucidating their electrical outputs. In summary, the theoretical framework enhances our understanding of the giant magnetoelastic effect in soft systems. It would provide an essential roadmap for the strategic design of future high-performance soft magnetoelastic devices.

MATERIALS AND METHODS

Fabrication of different magnetoelastic systems

Soft magnetoelastic systems were fabricated by mixing NdFeB micromagnets (5 μm) with the Ecoflex 00-30 (Smooth-on Inc.). The micromagnet volume concentrations were controlled to be 3.22, 6.25, 11.76, 21.05, and 28.57%. These micromagnet volume concentrations correspond to micromagnet-to-polymer ratios of 1:4, 1:2, 1:1, 2:1, and 3:1, respectively. For compression deformation, cylindrical and cuboidal magnetoelastic systems were fabricated. The cylindrical system has a radius of 8.5 mm and a height of 5 mm. The cuboidal system's dimensions are set at 15 mm in both length and width, with a height of 5 mm. For the local compression experiment, the cylindrical system with a micromagnet volume concentration of 11.76% is used. For stretch deformation experiments, cuboidal systems with two and three alternating magnetization domains are fabricated. The length, width, and height of the system are set to be 44, 15, and 2 mm, respectively. A lattice-structured magnetoelastic system is also fabricated with its specific dimension and micro-CT displayed in fig. S16. All the soft magnetoelastic systems are magnetized using impulse magnetization at ~2.6 T. Given the linear relationship between magnetization and particle volume concentration, it is reasonable to infer that all the systems under investigation are in their magnetically saturated states.

Simulation of magnetoelastic effects in soft systems

Air space was simulated using a spherical space with a radius of 40 mm together with infinite elements. Arbitrary Lagrangian-Eulerian formulations were used in the model to ensure accuracy. The total second Piola-Kirchhoff stress and boundary Maxwell stress were input manually into the model. When simulating the influence of magnetic force on the initial geometry of the sample, we have used weak constraints according to the symmetry of the geometry and magnetization distribution of the samples. When comparing simulation results with analytical results, we have excluded the contribution of magnetic force. The nonsmoothness in the generated voltage signals originates from irregularities in the magnetic flux-stretch curves, which result from the automatic remeshing during the simulation process.

Fabrication of the MI layer

The MI layer was fabricated on a flexible printed circuit board using patterned conductive traces of copper. The MI layer features an in-plane square coil with 90 turns: 45 turns on the top side of the polyimide substrate and 45 turns on the bottom side. The linewidth of the coil measures 76.2 μm, while the intercoil spacing is consistently maintained at 76.2 μm. Consequently, the total surface area occupied by the coil is approximately 14 mm by 14 mm.

Characterization of the soft magnetoelastic systems and MEGs

The mechanical shear modulus and stretchability of the soft magnetoelastic systems are measured using an advanced force testing system (TCD-225, Chatillon) with dog bone sample geometry. The micro-CT image of the magnetic lattice was scanned at 80 kVp/140 μA with 500-ms exposure using a μCT scanner (HiCT) developed by the Crump Institute for Molecular Imaging at the University of California, Los Angeles (UCLA). The magnetic flux density versus applied stress curve of each soft magnetoelastic system was obtained using a customized instrument that integrates a force gauge and a three-axis magnetic hall sensor (MLX-90393). The magnetic hall sensor was modified through a photocurable resin and sandpapers to ensure a fully smooth and flat surface. For local compression deformation measurements, a rod-shaped magnetic hall sensor (Tunkia, TD8620) was used in conjunction with the force gauge. Each soft magnetoelastic system was characterized independently three times. In the MEG electrical output characterization, a shaker (HT-126) was used to apply a sinusoidal compression deformation to the tested MEG. Short-circuit current signals were measured by a current preamplifier (SR570, Stanford Research). Open-circuit voltage signals were measured by an electrometer (Keithley 6514). A resistance box is used to evaluate the MEG's electrical output across varying external loads ranging from 1 to 1000 ohms. The MEG's power output is determined on the basis of the measured voltage and current for these respective loads.

Supplementary Materials

This PDF file includes:

Figs. S1 to S41
Tables S1 to S3
Notes S1 to S14
References

REFERENCES AND NOTES

1. E. R. Callen, H. B. Callen, Static magnetoelastic coupling in cubic crystals. *Phys. Rev.* **129**, 578–593 (1963).
2. M. J. Dapino, R. C. Smith, F. T. Calkins, A. B. Flatau, A coupled magnetomechanical model for magnetostrictive transducers and its application to Villari-effect sensors. *J. Intell. Mater. Syst. Struct.* **13**, 737–747 (2002).
3. L. Sandlund, M. Fahlander, T. Cedell, A. E. Clark, J. B. Restorff, M. Wun-Fogle, Magnetostriction, elastic moduli, and coupling factors of composite Terfenol-D. *J. Appl. Phys.* **75**, 5656–5658 (1994).
4. R. Szewczyk, A. Bieńkowski, Magnetoelastic Villari effect in high-permeability Mn-Zn ferrites and modeling of this effect. *J. Magn. Magn. Mater.* **254-255**, 284–286 (2003).
5. Z.-W. Fang, Y.-W. Zhang, X. Li, H. Ding, L.-Q. Chen, Integration of a nonlinear energy sink and a giant magnetostrictive energy harvester. *J. Sound Vib.* **391**, 35–49 (2017).
6. Z. Deng, M. J. Dapino, Review of magnetostrictive materials for structural vibration control. *Smart Mater. Struct.* **27**, 113001 (2018).
7. Y. Zhou, X. Zhao, J. Xu, Y. Fang, G. Chen, Y. Song, S. Li, J. Chen, Giant magnetoelastic effect in soft systems for bioelectronics. *Nat. Mater.* **20**, 1670–1676 (2021).
8. X. Zhao, Y. Zhou, J. Xu, G. Chen, Y. Fang, T. Tat, X. Xiao, Y. Song, S. Li, J. Chen, Soft fibers with magnetoelasticity for wearable electronics. *Nat. Commun.* **12**, 6755 (2021).
9. X. Zhao, A. Nashalian, I. W. Ock, S. Popoli, J. Xu, J. Yin, T. Tat, A. Libanori, G. Chen, Y. Zhou, J. Chen, A soft magnetoelastic generator for wind-energy harvesting. *Adv. Mater.* **34**, e2204238 (2022).
10. A. Libanori, J. Soto, J. Xu, Y. Song, J. Zarubova, T. Tat, X. Xiao, S. Z. Yue, S. J. Jonas, S. Li, J. Chen, Self-powered programming of fibroblasts into neurons via a scalable magnetoelastic generator array. *Adv. Mater.* **35**, e2206933 (2023).
11. I. W. Ock, X. Zhao, T. Tat, J. Xu, J. Chen, Harvesting hydropower via a magnetoelastic generator for sustainable water splitting. *ACS Nano* **16**, 16816–16823 (2022).
12. A. Saber, R. Sedaghati, The modeling of magnetorheological elastomers: A state-of-the-art review. *Adv. Eng. Mater.* **25**, 2300182 (2023).
13. T. A. Nadzharyan, M. Shamonin, E. Y. Kramarenko, Theoretical modeling of magnetoactive elastomers on different scales: A state-of-the-art review. *Polymers.* **14**, 4096 (2022).
14. Y.-S. Zhan, C.-h. Lin, A constitutive model of coupled magneto-thermo-mechanical hysteresis behavior for giant magnetostrictive materials. *Mech. Mater.* **148**, 103477 (2020).
15. Y.-S. Zhan, C.-h. Lin, Micromechanics-based constitutive modeling of magnetostrictive 1–3 and 0–3 composites. *Compos. Struct.* **260**, 113264 (2021).
16. C.-h. Lin, Y.-S. Zhan, Z. Deng, Constitutive modeling of oriented and non-oriented magnetostrictive particulate composites. *Compos. Struct.* **311**, 116781 (2023).
17. T. Mori, K. Tanaka, Average stress in matrix and average elastic energy of materials with misfitting inclusions. *Acta Metall.* **21**, 571–574 (1973).
18. Z. Deng, Explicit and efficient discrete energy-averaged model for Terfenol-D. *J. Appl. Phys.* **122**, 043901 (2017).
19. S. V. Kankanala, N. Triantafyllidis, On finitely strained magnetorheological elastomers. *J. Mech. Phys. Solids* **52**, 2869–2908 (2004).
20. Y.-H. Pao, Electromagnetic forces in deformable continua. *Mech. Today* **4**, 209–305 (1978).
21. A. Dorfmann, R. W. Ogden, Magnetoelastic modelling of elastomers. *Eur. J. Mech. A/Solids* **22**, 497–507 (2003).
22. A. Dorfmann, R. W. Ogden, Some problems in nonlinear magnetoelasticity. *Z. Angew. Math. Phys.* **56**, 718–745 (2005).
23. A. Dorfmann, R. W. Ogden, Nonlinear magnetoelastic deformations of elastomers. *Acta Mech.* **167**, 13–28 (2004).
24. W. F. Brown, *Magnetoelastic Interactions* (Springer, 1966), vol. 9.
25. G. A. Maugin, A. C. Eringen, Deformable magnetically saturated media. I. field equations. *J. Math. Phys.* **13**, 143–155 (1972).
26. G. A. Maugin, *Continuum Mechanics of Electromagnetic Solids* (Elsevier, 2013).
27. K. Danas, S. V. Kankanala, N. Triantafyllidis, Experiments and modeling of iron-particle-filled magnetorheological elastomers. *J. Mech. Phys. Solids* **60**, 120–138 (2012).
28. O. Stolbov, Y. Raikher, Large-scale shape transformations of a sphere made of a magnetoactive elastomer. *Polymers.* **12**, 2933 (2020).
29. O. V. Stolbov, Y. L. Raikher, Deformation of a sphere made of magnetoactive elastomer under a strong uniform magnetic field. *J. Phys. Conf. Ser.* **1945**, 012056 (2021).
30. Y. Kim, H. Yuk, R. Zhao, S. A. Chester, X. Zhao, Printing ferromagnetic domains for untethered fast-transforming soft materials. *Nature* **558**, 274–279 (2018).
31. R. Zhao, Y. Kim, S. A. Chester, P. Sharma, X. Zhao, Mechanics of hard-magnetic soft materials. *J. Mech. Phys. Solids* **124**, 244–263 (2019).
32. L. Wang, Y. Kim, C. F. Guo, X. Zhao, Hard-magnetic elastica. *J. Mech. Phys. Solids* **142**, 104045 (2020).
33. D. Yan, B. F. G. Aymon, P. M. Reis, A reduced-order, rotation-based model for thin hard-magnetic plates. *J. Mech. Phys. Solids* **170**, 105095 (2023).
34. Y. Kim, G. A. Parada, S. Liu, X. Zhao, Ferromagnetic soft continuum robots. *Sci. Robot.* **4**, eaax7329 (2019).

35. Y. Kim, E. Genevriere, P. Harker, J. Choe, M. Balicki, R. W. Regenhardt, J. E. Vranic, A. A. Dmytriw, A. B. Patel, X. Zhao, Telerobotic neurovascular interventions with magnetic manipulation. *Sci. Robot.* **7**, eabg9907 (2022).
36. L. Wang, D. Zheng, P. Harker, A. B. Patel, C. F. Guo, X. Zhao, Evolutionary design of magnetic soft continuum robots. *Proc. Natl. Acad. Sci. U.S.A.* **118**, e2021922118 (2021).
37. D. Mukherjee, M. Rambausek, K. Danas, An explicit dissipative model for isotropic hard magnetorheological elastomers. *J. Mech. Phys. Solids* **151**, 104361 (2021).
38. L. Dorfmann, R. W. Ogden, The nonlinear theory of magnetoelasticity and the role of the maxwell stress: A review. *Proc. R. Soc. A* **479**, 20230592 (2023).
39. C. Rinaldi, H. Brenner, Body versus surface forces in continuum mechanics: Is the maxwell stress tensor a physically objective cauchy stress? *Phys. Rev. E* **65**, 036615 (2002).
40. S. Ahmed, F. R. Jones, A review of particulate reinforcement theories for polymer composites. *J. Mater. Sci.* **25**, 4933–4942 (1990).
41. D. V. Redžić, Faraday's law via the magnetic vector potential. *Eur. J. Phys.* **28**, N7–N10 (2007).
42. H. Flanders, Differentiation under the integral sign. *Am. Math. Mon.* **80**, 615–627 (1973).
43. S. Lucarini, M. Hossain, D. Garcia-Gonzalez, Recent advances in hard-magnetic soft composites: Synthesis, characterisation, computational modelling, and applications. *Compos. Struct.* **279**, 114800 (2022).
44. A. Hoger, D. E. Carlson, On the derivative of the square root of a tensor and Guo's rate theorems. *J. Elast.* **14**, 329–336 (1984).
45. E. W. Lee, Magnetostriction and magnetomechanical effects. *Rep. Prog. Phys.* **18**, 184–229 (1955).
46. H.-Y. Chen, Y. Zhang, Y.-B. Yang, X.-G. Chen, S.-Q. Liu, C.-S. Wang, Y.-C. Yang, J.-B. Yang, Magnetostrictions and magnetic properties of Nd-Fe-B and $SrFe_{12}O_{19}$. *Chin. Phys. Lett.* **28**, 077501 (2011).
47. C. Graham, P. Flanders, High-field magnetostriction measurements on $Fe_{14}Nd_2B$ magnets. *IEEE Trans. Magn.* **22**, 749–751 (1986).

Acknowledgments: We acknowledge the Henry Samueli School of Engineering and Applied Science and the Department of Bioengineering at the UCLA for startup support. We acknowledge Y. Zhou for helpful discussions. **Funding:** J.C. acknowledges the Vernroy Makoto Watanabe Excellence in Research Award at the UCLA Samueli School of Engineering. This work was supported by the Office of Naval Research Young Investigator Award (award ID: N00014-24-1-2065), National Institutes of Health Grant (award ID: R01 CA287326), National Science Foundation Grant (award number: 2425858), the American Heart Association Innovative Project Award (award ID: 23IPA1054908), the American Heart Association Transformational Project Award (award ID: 23TPA1141360), the American Heart Association's Second Century Early Faculty Independence Award (award ID: 23SCEFIA1157587), the Brain and Behavior Research Foundation Young Investigator Grant (grant number: 30944), and the NIH National Center for Advancing Translational Science UCLA CTSI (grant number: KL2TR001882). **Author contributions:** Conceptualization: Y.Z., J.C., G.C., and X.Z. Theory development and finite element implementation: Y.Z. and J.C. Experiments: Y.Z., G.C., and X.Z. Visualization: Y.Z., X.Z., and J.C. Funding acquisition: J.C. Project administration: J.C. Supervision: J.C. Writing—original draft: Y.Z.. and J.C. Writing—review and editing: Y.Z., G.C., X.Z., T.T., Z.D., and J.C. **Competing interests:** The authors declare that they have no competing interests. **Data and materials availability:** All data needed to evaluate the conclusions in the paper are present in the paper and/or the Supplementary Materials.

Submitted 25 July 2024
Accepted 2 December 2024
Published 3 January 2025
10.1126/sciadv.ads0071